

Role of the Ce valence in the coexistence of superconductivity and ferromagnetism of $\text{CeO}_{1-x}\text{F}_x\text{BiS}_2$ revealed by Ce L_3 -edge x-ray absorption spectroscopy

T. Sugimoto,¹ B. Joseph,² E. Paris,² A. Iadecola,³ T. Mizokawa,^{1,2,4} S. Demura,^{5,6} Y. Mizuguchi,⁷ Y. Takano,^{5,6} and N. L. Saini²

¹*Department of Complexity Science and Engineering, University of Tokyo, 5-1-5 Kashiwanoha, Chiba 277-8561, Japan*

²*Dipartimento di Fisica, Università di Roma “La Sapienza”–Piazzale Aldo Moro 2, 00185 Roma, Italy*

³*Elettra–Sincrotrone SCpAss 14-km 163.5 34149 Basovizza, Trieste, Italy*

⁴*Department of Physics, University of Tokyo, 5-1-5 Kashiwanoha, Chiba 277-8561, Japan*

⁵*National Institute for Materials Science, 1-2-1 Sengen, Tsukuba 305-0047, Japan*

⁶*Graduate School of Pure and Applied Science, University of Tsukuba, 1-1-1 Tennodai, Tsukuba 305-8577, Japan*

⁷*Department of Electrical and Electronic Engineering, Tokyo Metropolitan University, 1-1 Minami-osawa, Hachioji 192-0397, Japan*

(Received 14 March 2014; revised manuscript received 18 May 2014; published 30 May 2014)

We have performed Ce L_3 -edge x-ray absorption spectroscopy (XAS) measurements on $\text{CeO}_{1-x}\text{F}_x\text{BiS}_2$, in which the superconductivity of the BiS_2 layer and the ferromagnetism of the $\text{CeO}_{1-x}\text{F}_x$ layer are induced by the F doping, in order to investigate the impact of the F doping on the local electronic and lattice structures. The Ce L_3 -edge XAS spectrum of CeOBiS_2 exhibits coexistence of $4f^1$ (Ce^{3+}) and $4f^0$ (Ce^{4+}) state transitions revealing Ce mixed valency in this system. The spectral weight of the $4f^0$ state decreases with the F doping and completely disappears for $x > 0.4$ where the system shows the superconductivity and the ferromagnetism. The results suggest that suppression of the Ce-S-Bi coupling channel by the F doping appears to drive the system from the valence fluctuation regime to the Kondo-like regime, leading to the coexistence of the superconducting BiS_2 layer and the ferromagnetic $\text{CeO}_{1-x}\text{F}_x$ layer.

DOI: [10.1103/PhysRevB.89.201117](https://doi.org/10.1103/PhysRevB.89.201117)

PACS number(s): 74.25.Jb, 74.70.Xa, 78.70.Dm, 71.28.+d

Since the discovery of high- T_c superconductivity in layered Fe pnictides [1], tremendous research efforts have been dedicated to the exploration of new superconductors in various pnictides and chalcogenides with layered structures. Very recently, a new family of superconductors with a BiS_2 layer has been discovered by Mizuguchi *et al.* [2], and the discovery was followed by extensive research activity on related systems including $\text{REO}_{1-x}\text{F}_x\text{BiS}_2$ (RE = rare-earth elements) with the BiS_2 layer [3–16]. In $\text{REO}_{1-x}\text{F}_x\text{BiS}_2$, the electronically active BiS_2 layers are separated by the REO spacers, and the band filling and the superconductivity of the BiS_2 layer can be controlled by the F doping in the REO spacers. The maximum T_c of 10.5 K has been achieved in $\text{LaO}_{1-x}\text{F}_x\text{BiS}_2$ synthesized by high pressure annealing [6], whereas that synthesized at ambient pressure tends to be nonsuperconducting. In addition, high pressure studies on optimally doped $\text{LaO}_{0.5}\text{F}_{0.5}\text{BiS}_2$ (synthesized at ambient pressure) have revealed that T_c increases up to the maximum value of 10.1 K at 1–2 GPa followed by a gradual decrease with increasing pressure [17,18]. These experiments indicate that the superconductivity in BiS_2 -based superconductors is highly sensitive to the local atomic displacements.

While various BiS_2 -based systems have been synthesized with different spacer layers, the particular case of $\text{CeO}_{1-x}\text{F}_x\text{BiS}_2$ with coexistence of superconductivity and ferromagnetism at low temperature is interesting [19]. In fact, $\text{CeO}_{1-x}\text{F}_x\text{BiS}_2$ shows superconductivity and ferromagnetism with a maximum T_c of 6 K. While BiS_2 -based superconductors have been considered as conventional superconductors with electron-phonon coupling, the coexistence of superconductivity and ferromagnetism provokes further studies to understand the interaction of different electronic degrees of freedom and the role of spacer layers in these materials. In addition, the ferromagnetism and the superconductivity are enhanced in the

samples synthesized by high pressure annealing, indicating high sensitivity to the local atomic displacements.

Ce L_3 x-ray absorption spectroscopy (XAS) is a direct probe of the local structure around a selected absorbing atom and distribution of the valence electrons, with the final states in the continuum being due to multiple scattering resonances of the photoelectron in a finite cluster [20]. In this work, we have exploited Ce L_3 XAS to investigate the impact of the F doping on the local electronic and lattice structures of a $\text{CeO}_{1-x}\text{F}_x\text{BiS}_2$ system synthesized differently, i.e., as grown (AG) and high pressure (HP) annealed. Since it is difficult to prepare clean surfaces using the available polycrystalline $\text{CeO}_{1-x}\text{F}_x\text{BiS}_2$ samples, the bulk-sensitive Ce L_3 -edge XAS taken in the transmission mode is the most reliable tool to evaluate the Ce valence. The Ce L_3 -edge XAS spectrum of CeOBiS_2 exhibits the transitions to the $4f^1$ and $4f^0$ final states, indicating the $\text{Ce}^{3+}/\text{Ce}^{4+}$ valence fluctuation that should be related to the Ce-S-Bi coupling channel. Namely, the Ce^{3+} ($4f^1$) and Ce^{4+} ($4f^0$) states are mixed in the ground state due to the hybridization between the Ce $4f$ orbitals and the Bi $6p$ conduction band. The spectral weight of the $4f^0$ states decreases with the F doping and disappears completely for $x > 0.4$ where the system shows the coexistence of the superconductivity and ferromagnetism at low temperature. The F doping is expected to break the Ce-S-Bi coupling channel and induce crossover from the valence fluctuation regime to the Kondo-like regime.

Ce L_3 -edge XAS measurements were performed on polycrystalline samples of $\text{CeO}_{1-x}\text{F}_x\text{BiS}_2$ prepared by the solid-state reaction method. Both AG and HP annealed samples were used for the measurements. All the samples were well characterized for their transport and average structural properties prior to the absorption measurements. Details on the sample preparation and characterization are given elsewhere [19].

The x-ray absorption experiments were performed at the XAFS beamline of the Elettra Synchrotron Radiation Facility, Trieste, where the synchrotron radiation emitted by a bending magnet source was monochromatized using a double crystal Si(111) monochromator. The measurements were taken at room temperature in transmission mode using three ionization chambers mounted in series for simultaneous measurements on the sample and a reference. As a routine experimental approach, several absorption scans were collected on each sample to ensure the reproducibility of the spectra, in addition to the high signal-to-noise ratio.

Figure 1 displays the Ce L_3 -edge XAS spectra of AG [Fig. 1(a)] and HP [Fig. 1(b)] $\text{CeO}_{1-x}\text{F}_x\text{BiS}_2$ ($x = 0.0, 0.2, 0.4, 0.6, 0.8,$ and 1.0). The spectra are normalized with respect to the atomic absorption estimated by a linear fit to the high energy part of the spectra. Three main structures around 5725, 5737, and 5758 eV can be identified on the Ce L_3 -edge XAS spectra. The first peak around 5725 eV is the absorption white line corresponding to the transition from the Ce $2p$ core level to the vacant Ce $5d$ state mixed with the Ce $4f^1$ final state [21–24]. On the other hand, the second peak around 5737 eV corresponds to the transition from the Ce $2p$ core level to the vacant Ce $5d$ state mixed with the Ce $4f^0$ final state.

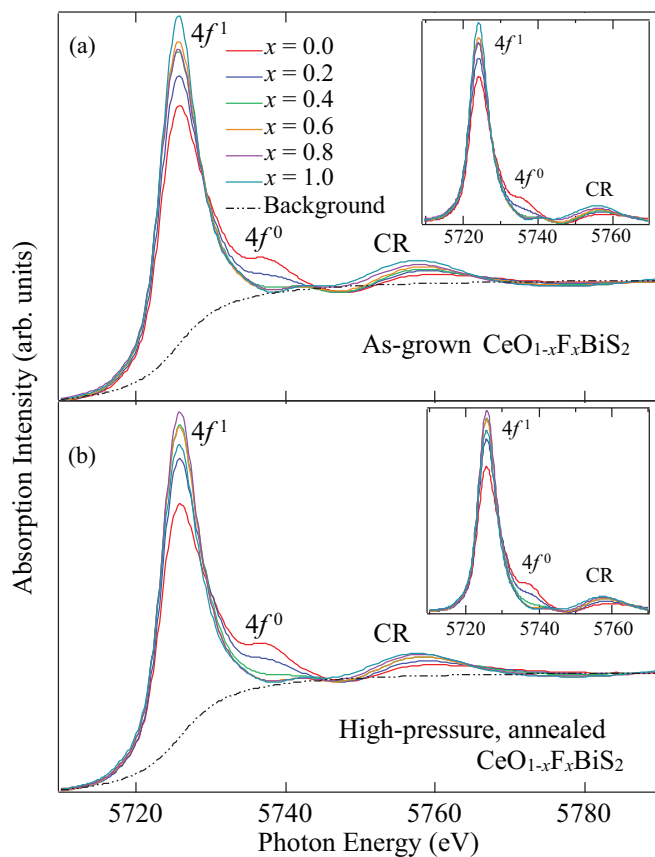


FIG. 1. (Color online) (a) Ce L_3 -edge normalized XAS spectra of AG and (b) HP $\text{CeO}_{1-x}\text{F}_x\text{BiS}_2$ with $x = 0.0, 0.2, 0.4, 0.6, 0.8,$ and 1.0 . The $4f^1$, $4f^0$, and CR peaks around 5725, 5737, and 5758 eV are shown. The background (arctangent function)-subtracted spectra are shown in the insets. The spectra were taken at room temperature with transmission mode.

The $4f^1$ and $4f^0$ final states are the so-called well-screened and poorly screened states and provide information on the Ce valence states. The presence of both $4f^1$ and $4f^0$ states suggest the $\text{Ce}^{3+}/\text{Ce}^{4+}$ valence fluctuation. On the other hand, the energy difference between the $4f^1$ and $4f^0$ absorption peaks, which is approximately 12 eV [21–23] is mainly determined by the Ce $2p$ -Ce $4f$ Coulomb interaction and is expected to be independent of the F doping. One can see a systematic change due to the F doping in the $4f^1$ and $4f^0$ peak intensity. The third peak around 5758 eV includes the information on the local lattice structures. This peak is the so-called continuum resonance (CR), likely to be due to Ce-Bi scattering with a

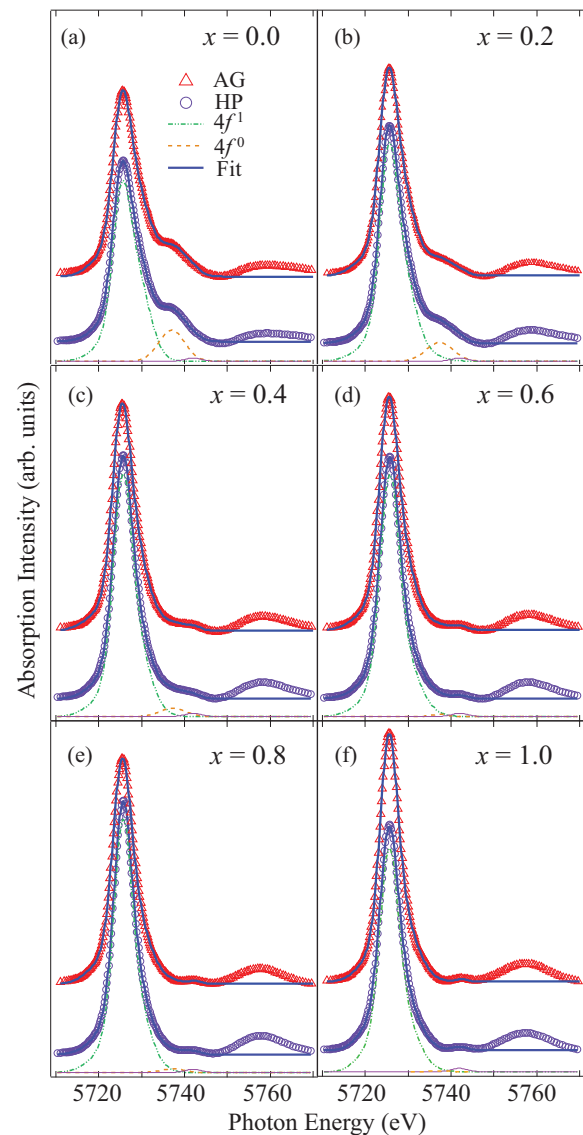


FIG. 2. (Color online) Multicurve fitting results on Ce L_3 -edge XAS spectra in $\text{CeO}_{1-x}\text{F}_x\text{BiS}_2$ with (a) $x = 0.0$, (b) $x = 0.2$, (c) $x = 0.4$, (d) $x = 0.6$, (e) $x = 0.8$, and (f) $x = 1.0$. The experimental data of AG and HP are shown as triangles and circles, respectively. The fitted results are shown by solid lines on the HP and AG experimental data. Each component of the fitting lines is shown only for the HP experimental data. The tiny peak around 5742 eV is fixed for all the cases from (a) to (f).

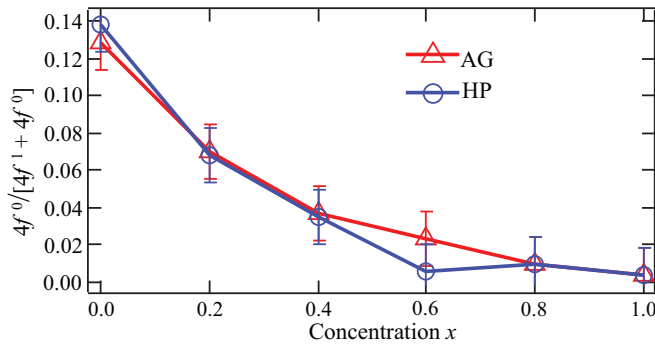


FIG. 3. (Color online) The relative spectral weight of $4f^0$ states for both AG and HP samples.

contribution from the Ce-Ce scattering, reflecting evolution of the Ce-Bi/Ce bond length. In addition, there is a weak feature around 5742 eV. This feature is a characteristic feature of layered rare-earth systems, and its intensity is generally sensitive to the O/F atom order/disorder in the CeO/F layer.

In order to qualify the electronic states, we have estimated the spectral weight of $4f^1$ and $4f^0$ absorption peaks using the following procedure. A constant background estimated by an arctangent function was subtracted from the XAS spectra (inset of Fig. 1). The background-subtracted spectra were fitted by Gaussian functions, reproducing all the main peaks, i.e., $4f^1 + 4f^0$ as shown in Fig. 2. As for the $4f^1$ peak, we utilized three Gaussian functions to reproduce the asymmetric line shape, while a symmetric Gaussian function was enough to describe the $4f^0$ peak. The $4f^0$ peak is found to decrease monotonically with the F doping. The fit of the weak peak (peak around 5742 eV, a characteristic feature of layered structures) is fixed for all the fits since this feature is independent of the F doping. The weak peak was used in the fit in order to ensure the proper area estimation of the $4f^0$ peak. The CR was not considered

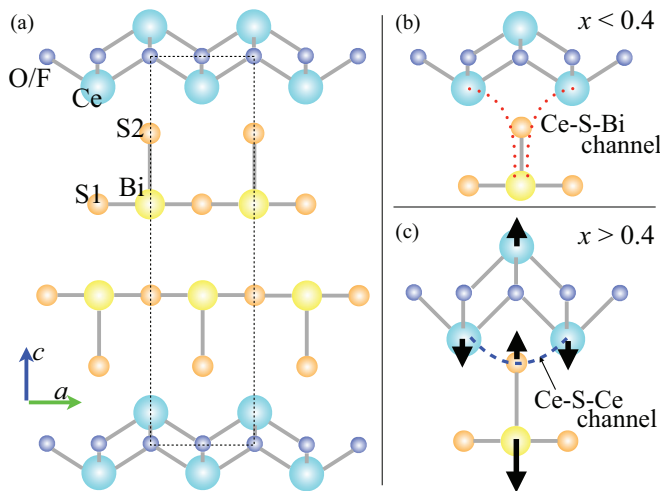


FIG. 4. (Color online) (a) The crystal structure of $\text{CeO}_{1-x}\text{F}_x\text{BiS}_2$. The dashed box represents the unit cell. (b) The local structure of $\text{CeO}_{1-x}\text{F}_x\text{BiS}_2$ for $x < 0.4$ and (c) for $x > 0.4$. The bond length of Ce-S2 decreases and that of Bi-S2 increases when $x > 0.4$ as depicted.

in the fit. The fits for all the samples are shown along with the experimental results.

The intensity of the main peaks $4f^1 + 4f^0$ depends on the amount of additional background from the grain boundaries and the hybridization between the Ce $4f$ and Ce $5d$ orbitals which can be changed by the F doping and the high pressure synthesis. Therefore, we employ the relative spectral weight $4f^0/[4f^1 + 4f^0]$, which is obtained by integrating the Gaussian functions and is shown in Fig. 3, in order to discuss the Ce valence. The relatively large $4f^0/[4f^1 + 4f^0]$ value in CeOBiS_2 indicates that the Ce^{4+} state with $4f^0$ electronic configuration is coexisting with the Ce^{3+} state with $4f^1$ electronic configuration [19,21,22]. The existence of the $4f^0$ peak, namely, the valence fluctuation between the Ce^{3+} and Ce^{4+} states in CeOBiS_2 , is in sharp contrast to the pure Ce^{3+} state in iron-based CeOFeAs pnictides [24,25]. The $4f^0/[4f^1 + 4f^0]$ value decreases with the F doping both in the AG and HP samples. The $4f^0/[4f^1 + 4f^0]$ value of the AG sample is slightly larger than the HP sample at $x = 0.6$, which is located between the $\text{Ce}^{3+}/\text{Ce}^{4+}$ valence fluctuation regime and the Ce^{3+} Kondo-like regime. The small $4f^0/[4f^1 + 4f^0]$ value at $x = 0.6$ in the HP sample

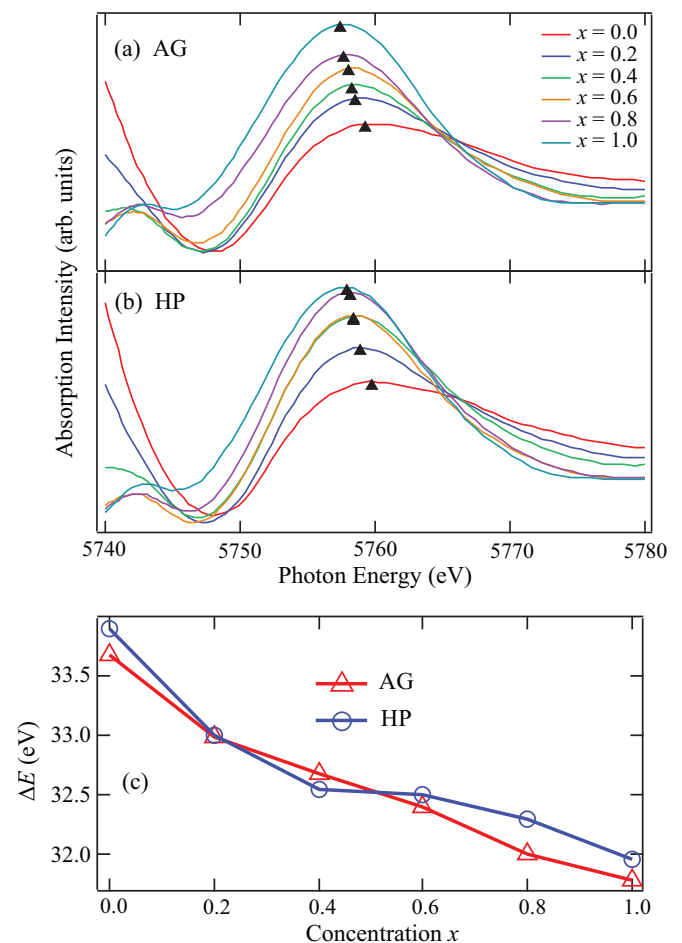


FIG. 5. (Color online) Evolution of the CR as a function of the F doping in (a) AG samples and (b) HP samples. Peak positions are indicated by small triangles. (c) Changes of the energy relative to the absorption white line (ΔE) as a function of the F doping.

would be consistent with the fact that the superconductivity and ferromagnetism tend to be enhanced in the HP samples. However, the difference in $4f^0/[4f^1 + 4f^0]$ is very subtle, suggesting that some additional factors such as inhomogeneity play an important role in the difference between the AG and HP samples.

Recalling the atomic structure, the layered structure of CeOBiS₂ contains a BiS₂ layer intercalated with a CeO layer. The in-plane S atoms in the BiS₂ layer [S1 as in Fig. 4(a)] are located at a distance of about 2.8 Å from the Bi atoms, while the out-of-plane S [S2 as in Fig. 4(a)] atom linking the spacer layer with the BiS₂ plane is located at a distance of about 2.6 Å. By the F substitution, the Bi-S2 distance increases ($\Delta R_{\max} \sim 0.12$ Å), while the Ce-S2 distance decreases ($\Delta R_{\max} \sim 0.15$ Å) [19,26], leading to breaking of the Ce-S-Bi coupling channel as in Figs. 4(b) and 4(c). Consequently, the hybridization between the Ce 4*f* orbital and the Bi 6*p* conduction band decreases with the F doping and the Ce³⁺/Ce⁴⁺ valence fluctuation is suppressed. This means that the F doping drives the system from the Ce³⁺/Ce⁴⁺ valence fluctuation regime to the Ce³⁺ Kondo-like regime [22]. Indeed, the Ce 4*f*⁰ spectral weight almost disappears at $x > 0.4$, where the system shows the superconductivity and the ferromagnetism. Therefore, it seems that the mixed valence of Ce, namely, the coupling between the Ce 4*f* and Bi 6*p* states, is not good for the superconducting state. The Ce 4*f* electrons are localized in the Kondo regime for $x > 0.4$ and that should be responsible for the ferromagnetism. The ferromagnetic Ce compounds in the Kondo regime are rather uncommon [27–33] and the direct Ce-Ce exchange interaction plays an important role in many cases. In CeO_{1-x}F_xBiS₂, the Ce-Ce distance is relatively longer than the ferromagnetic Ce compounds. Therefore, instead of the direct Ce-Ce exchange interaction, the Ce-S-Ce superexchange interaction as in Fig. 4(c) between Ce³⁺ sites is expected to be responsible for the ferromagnetism of the CeO_{1-x}F_x layer. For $x > 0.4$, the ferromagnetic CeO_{1-x}F_x layer is expected to be insulating just like the LaO_{1-x}F_x layer, and is decoupled from the superconducting BiS₂ layer.

The above arguments are consistent with the structural changes observed in the same experiment through the CR peak. The CR peak is due to the Ce-Bi scattering with a contribution from the Ce-Ce. Figure 5 shows a zoom over of the CR peak for the two series of CeO_{1-x}F_xBiS₂ samples, with the peak position evolving with the F doping. The decrease of energy separation between the white line and the CR peak suggests that the Ce-Bi distance becomes elongated following the empirical rule for the CR ($\Delta E \propto 1/d^2$) [20]. The elongation of the Ce-Bi bond length would contribute to the reduction of the Ce-Bi coupling through the Ce-S-Bi channel. Namely, the hybridization between the Ce 4*f* orbital and the Bi 6*p* conduction band decreases with the F doping and the Ce³⁺/Ce⁴⁺ valence fluctuation is suppressed. This is consistent with the decrease of the $4f^0/[4f^1 + 4f^0]$ value by the F doping.

In conclusion, the Ce *L*₃-edge XAS results on CeO_{1-x}F_xBiS₂ show that the superconductivity and ferromagnetism are suppressed for $x < 0.4$ in the valence fluctuation regime evidenced by the 4*f*¹ and 4*f*⁰ states. The peak position of the CR depends on the F doping and indicates that the Ce-Bi bond length increases with the F doping. The present experimental results show that CeOBiS₂ has the Ce³⁺/Ce⁴⁺ valence fluctuation due to the Ce-Bi coupling through the Ce-S-Bi channel and that the superconductivity of the BiS₂ layer tends to be suppressed by the Ce-Bi coupling. The Ce-S-Bi coupling channel is broken by the F doping. Consequently, the system undergoes a crossover from the valence fluctuation regime for $x < 0.4$ to the Kondo-like regime for $x > 0.4$ in which the superconducting BiS₂ layer and the ferromagnetic CeO_{1-x}F_x layer are decoupled and hence coexist. The results provide important information on the role of Ce valence in the coexisting superconductivity and ferromagnetism in the CeO_{1-x}F_xBiS₂ system.

The present work is a part of the bilateral agreement between the Sapienza University of Rome and the University of Tokyo, and is partly supported by a Grant-in-Aid for Scientific Research from the Japan Society for Promotion of Science.

-
- [1] Y. Kamihara, T. Watanabe, M. Hirano, and H. Hosono, *J. Am. Chem. Soc.* **130**, 3296 (2008).
- [2] Y. Mizuguchi, H. Fujihisa, Y. Gotoh, K. Suzuki, H. Usui, K. Kuroki, S. Demura, Y. Takano, H. Izawa, and O. Miura, *Phys. Rev. B* **86**, 220510(R) (2012).
- [3] S. K. Singh, A. Kumar, B. Gahtori, S. Kirtan, G. Sharma, S. Patnaik, and V. P. S. Awana, *J. Am. Chem. Soc.* **134**, 16504 (2012).
- [4] B. Li, Z. W. Xing, and G. Q. Huang, *Europhys. Lett.* **101**, 47002 (2013).
- [5] K. Deguchi, Y. Mizuguchi, S. Demura, H. Hara, T. Watanabe, S. J. Denholme, M. Fujioka, H. Okazaki, T. Ozaki, H. Takeya, T. Yamaguchi, O. Miura, and Y. Takano, *Europhys. Lett.* **101**, 17004 (2013).
- [6] H. Kotegawa, Y. Tomita, H. Tou, H. Izawa, Y. Mizuguchi, O. Miura, S. Demura, K. Deguchi, and Y. Takano, *J. Phys. Soc. Jpn.* **81**, 103702 (2012).
- [7] S. Demura, Y. Mizuguchi, K. Deguchi, H. Okazaki, H. Hara, T. Watanabe, S. J. Denholme, M. Fujioka, T. Ozaki, H. Fujihisa, Y. Gotoh, O. Miura, T. Yamaguchi, H. Takeya, and Y. Takano, *J. Phys. Soc. Jpn.* **82**, 033708 (2013).
- [8] V. P. S. Awana, A. Kumar, R. Jha, S. K. Singh, A. Pal, Shrutti, J. Saha, and S. Patnaik, *Solid State Commun.* **157**, 21 (2013).
- [9] R. Jha, A. Kumar, S. K. Singh, and V. P. S. Awana, *J. Appl. Phys.* **113**, 056102 (2013).
- [10] J. Xing, S. Li, X. Ding, H. Yang, and H.-H. Wen, *Phys. Rev. B* **86**, 214518 (2012).
- [11] D. Yazici, K. Huang, B. D. White, A. H. Chang, A. J. Friedman, and M. B. Maple, *Philos. Mag.* **93**, 673 (2012).
- [12] D. Yazici, K. Huang, B. D. White, I. Jeon, V. W. Burnett, A. J. Friedman, I. K. Lum, M. Nallaiyan, S. Spagna, and M. B. Maple, *Phys. Rev. B* **87**, 174512 (2013).
- [13] T. Yildirim, *Phys. Rev. B* **87**, 020506(R) (2013).

- [14] Y. Liang, X. Wu, W-F. Tsai, and J. Hu, *Front. Phys.* **9**, 194 (2014).
- [15] X. Wan, H. C. Ding, S. Y. Savrasov, and C. G. Duan, *Phys. Rev. B* **87**, 115124 (2013).
- [16] J. Lee, M. B. Stone, A. Huq, T. Yildirim, G. Ehlers, Y. Mizuguchi, O. Miura, Y. Takano, K. Deguchi, S. Demura, and S.-H. Lee, *Phys. Rev. B* **87**, 205134 (2013).
- [17] C. T. Wolowiec, D. Yazici, B. D. White, K. Huang, and M. B. Maple, *Phys. Rev. B* **88**, 064503 (2013).
- [18] G. Kalai Selvan, M. Kanagaraj, S. Esakki Muthu, R. Jha, V. P. S. Awana, and S. Arumugam, *Phys. Status Solidi RRL* **7**, 510 (2013).
- [19] S. Demura, K. Deguchi, Y. Mizuguchi, K. Sato, R. Honjyo, A. Yamashita, T. Yamaki, H. Hara, T. Watanabe, S. J. Denholme, M. Fujioka, H. Okazaki, T. Ozaki, O. Miura, T. Yamaguchi, H. Takeya, and Y. Takano, [arXiv:1311.4267](https://arxiv.org/abs/1311.4267).
- [20] A. Bianconi, M. Dell'Aricecia, A. Gargano, and C. R. Natoli, in *EXAFS and Near Edge Structure*, edited by A. Bianconi, L. Incoccia, and S. Stipcich (Springer-Verlag, Berlin, 1983), pp. 57–61; A. Bianconi, E. Fritsch, G. Calas, and J. Petiau, *Phys. Rev. B* **32**, 4292 (1985).
- [21] B. T. Thole, G. van der Laan, J. C. Fuggle, G. A. Sawatzky, R. C. Karnatak, and J.-M. Esteve, *Phys. Rev. B* **32**, 5107 (1985).
- [22] H. Matsuyama, I. Harada, and A. Kotani, *J. Phys. Soc. Jpn.* **66**, 337 (1997).
- [23] A. Kotani, K. O. Kvashnina, P. Glatzel, J. C. Parlebas, and G. Schmerber, *Phys. Rev. Lett.* **108**, 036403 (2012).
- [24] T. Kroll, F. Roth, A. Koitzsch, R. Kraus, D. R. Batchelor, J. Werner, G. Behr, B. Büchner, and M. Knupfer, *New J. Phys.* **11**, 025019 (2009).
- [25] F. Bondino, E. Magnano, C. H. Booth, F. Offi, G. Panaccione, M. Malvestuto, G. Paolicelli, L. Simonelli, F. Parmigiani, M. A. McGuire, A. S. Sefat, B. C. Sales, R. Jin, P. Vilmercati, D. Mandrus, D. J. Singh, and N. Mannella, *Phys. Rev. B* **82**, 014529 (2010).
- [26] E. Paris, B. Joseph, A. Iadecola, T. Sugimoto, L. Olivi, S. Demura, Y. Mizuguchi, Y. Takano, T. Mizokawa, and N. L. Saini (unpublished).
- [27] H. J. Van Daal and K. H. J. Buschow, *Phys. Lett. A* **31**, 103 (1970).
- [28] R. Takke, N. Dolezal, W. Assmus, and B. Lüthi, *J. Magn. Magn. Mater.* **23**, 247 (1981).
- [29] S. K. Dhar, S. K. Malik, and R. Vijayaraghavan, *J. Phys. C* **14**, L321 (1981).
- [30] M. Jerjini, M. Bonnet, P. Burlet, G. Lapertot, J. Rossat-Mignod, J. Y. Henry, and D. Gignoux, *J. Magn. Magn. Mater.* **76-77**, 405 (1988).
- [31] K. Abe, J. Kitagawa, N. Takeda, and M. Ishikawa, *Phys. Rev. Lett.* **83**, 5366 (1999).
- [32] S. Raymond, P. Haen, R. Calemczuk, S. Kambe, B. Fåk, P. Lejay, T. Fukuhara, and J. Flouquet, *J. Phys.: Condens. Matter* **11**, 5547 (1999).
- [33] P. Manfrinetti, S. K. Dhar, R. Kulkarni, and A. V. Morozkin, *Solid State Commun.* **135**, 444 (2005).